

RESEARCH ARTICLE

Constitutively active mTORC1 signaling modifies the skeletal muscle metabolome and lipidome response to exercise

Hanna Kalenta,^{1,4} Sean P. Kilroe,^{1,4} Trevor B. Romsdahl,^{2,4} Erik D. Marchant,^{1,4} Rosario Maroto,² Jennifer J. Linares,^{2,3} William K. Russell,^{2,3} and Blake B. Rasmussen^{1,4}

¹Department of Cellular and Integrative Physiology, University of Texas Health Science Center at San Antonio, San Antonio, Texas, United States; ²Department of Biochemistry and Molecular Biology, University of Texas Medical Branch, Galveston, Texas, United States; ³Mass Spectrometry Facility, University of Texas Medical Branch, Galveston, Texas, United States; and ⁴Barshop Institute for Longevity and Aging Studies, University of Texas Health Science Center at San Antonio, San Antonio, Texas, United States

Abstract

A chronic increase in the Mammalian Target of Rapamycin Complex 1 (mTORC1) signaling is implicated in reduced longevity, altered metabolism, and mitochondrial dysfunction. Abnormal mTORC1 signaling may also be involved in the etiology of sarcopenia. To better understand the role of mTORC1 signaling in the regulation of muscle metabolism, we developed an inducible muscle-specific knockout model of DEP domain-containing 5 protein (DEPDC5 mKO), which results in constitutively active mTORC1 signaling. We hypothesized that constitutively active mTORC1 signaling in skeletal muscle would alter the metabolomic and lipidomic response to an acute bout of exercise. Wild-type (WT) and DEPDC5 muscle-specific knockout (KO) mice were studied at rest and following a 1 h bout of treadmill exercise. Acute exercise induced an increased reliance on glycolytic and pentose phosphate pathway (PPP) metabolites in the muscle of mice with hyperactive mTORC1. Lipidomic analysis showed an increase in triglycerides (TGs) in KO mice. Although exercise had a pronounced effect on muscle metabolism, the genotype effect was larger, indicating that constitutively active mTORC1 signaling exerts a dominant influence on metabolic and lipidomic regulation. We conclude that increased mTORC1 signaling shifts muscle metabolism toward greater reliance on nonoxidative energy sources in response to exercise. Understanding the mechanisms responsible for these effects may lead to the development of strategies for restoring proper mTORC1 signaling in conditions such as aging and sarcopenia.

NEW & NOTEWORTHY This study demonstrates that hyperactive mTORC1 alters the muscle metabolomic and lipidomic response to exercise, with genotype having a larger effect than exercise. Knockout mice exhibited an increase in reliance on glycolysis and pentose phosphate pathway and an increase in triglyceride turnover. Wild-type mice primarily showed an increase in utilization of TCA cycle and lipid metabolism intermediates.

exercise; lipidomics; metabolomics; mTORC1; muscle

INTRODUCTION

Mammalian target of rapamycin (mTOR) is a 289-kDa serine/threonine protein kinase and a member of the phosphatidylinositol 3-kinase-related kinase (PIKK) family. It consists of two distinct protein complexes: mTOR Complex 1 (mTORC1) and mTOR Complex 2 (mTORC2). mTORC1 is an important regulator of cellular growth and proliferation. It participates in balancing catabolism and anabolism through lipid, nucleotide, and protein synthesis, autophagy, lysosome biogenesis, and can be regulated by amino acid availability, growth factors, energy status, and mechanical stimuli, such as exercise and muscle contraction (1, 2). Short-term mTORC1 activation plays a beneficial role in maintaining cellular homeostasis, whereas chronic activation can disrupt normal metabolic regulation (1). Chronic

activation of mTORC1 is associated with disrupted insulin signaling, dysregulated translation initiation and ribosomal biogenesis, lipid accumulation, and inhibition of autophagy, all of which contribute to alterations in carbohydrate, protein, and lipid metabolism (3, 4). The role of chronic mTORC1 activation in reducing longevity is recognized, and studies have also shown that chronic mTORC1 activation can be linked to sarcopenia, an age-related involuntary loss of skeletal muscle mass and function (5, 6). The potential causes of sarcopenia are not completely understood but are related to an increased number of proinflammatory cytokines and an age-related increase in mitochondrial dysfunction (7, 8). Although the exact mechanism of dysregulated mTORC1 in aging is unknown, chronically active mTORC1 has been associated with the inhibition of autophagy and fiber damage in skeletal muscle (6, 9).



Correspondence: B. B. Rasmussen (rasmussenb@uthscsa.edu).

Submitted 17 December 2024 / Revised 21 January 2025 / Accepted 4 April 2025



A single bout of exercise drives transient changes in the skeletal muscle by altering mTORC1 activity and gene transcription and carbohydrate, lipid, and mitochondrial metabolism (10). These changes are based on the type of exercise (resistance or endurance), exercise intensity (low, medium, and high), duration, sex, age, diet, and training status (11). However, it is not known how an acute bout of exercise affects skeletal muscle with chronically active mTORC1. Examining hyperactive mTORC1 in the context of acute exercise, a strong driver of metabolic changes in muscle, allows us to assess how persistent mTORC1 activation influences exercise-induced metabolic adaptations. This approach may provide insights into how excessive mTORC1 signaling alters muscle metabolism, helping to differentiate metabolic changes between a potentially diseased and healthy state.

The analysis of skeletal muscle metabolome and lipidome provides valuable insights into substrate utilization, mitochondrial function, and lipid-based regulatory processes, all of which are very important for understanding muscle health. Considering the impact of mTORC1 on metabolic pathways and lipid accumulation, characterizing the skeletal muscle metabolome and lipidome can help elucidate how chronic mTORC1 activation influences muscle metabolism. There are relatively few studies that have comprehensively examined the muscle metabolome after an acute (i.e., single) bout of prolonged (>45–60 min) endurance exercise in mice. One study found general changes in amino acid and purine/pyrimidine metabolic pathways in the skeletal muscle in mice after 1 h of an acute treadmill exercise (12). This study also reported an overall decrease in glycolytic metabolites and an increase in urea with exercise (12). Another study found increased urea cycle, citric acid cycle, alanine metabolism, arginine/proline, and malate-aspartate shuttle biochemical pathways after an acute bout of exercise to exhaustion in mice (13). However, most studies have focused on analyzing a small number of metabolites rather than providing a comprehensive analysis of the entire metabolome.

Similarly, relatively few studies have examined the skeletal muscle lipidome in response to acute exercise. One study examined the effects of an hour of treadmill exercise in mice and found no significant changes compared with rest (14). The previous research has focused mainly on lipids from plasma (15) or nonmuscle tissues (16) or has focused on exercise training rather than acute exercise (17). Furthermore, these studies used different mammalian species (e.g., mice and humans), which makes it difficult to compare them with each other. In addition, many studies have traditionally focused on changes in intramuscular triglycerides (IMTGs) with exercise without considering the broader interplay among other lipid classes (18, 19). By focusing on different lipid classes, we can gain a more comprehensive view of lipid metabolism in skeletal muscle and its interaction with mTORC1 signaling.

Previously, our laboratory found a significant increase in muscle mitochondrial function and alterations in muscle metabolism in mice with constitutively active muscle mTORC1 using an inducible skeletal muscle-specific knockout mouse of DEP domain-containing 5 protein (DEPDC5 mKO) (20, 21). Exercise is known to affect substrate utilization and metabolic pathways localized in

mitochondria. Therefore, we used metabolomics and lipidomics analyses to investigate the effects of a 1 h bout of treadmill exercise on skeletal muscle in DEPDC5 mKO mice. We hypothesized that constitutively active mTORC1 signaling in skeletal muscle would alter the metabolomic and lipidomic response to an acute bout of exercise. Our findings showed that acute exercise induced an increased reliance on glycolytic and pentose phosphate pathway (PPP) metabolites in the muscle of mice with hyperactive mTORC1. Lipidomic analysis showed an increase in triglycerides (TGs) in KO mice.

METHODS

Transgenic Mice and Skeletal Muscle Collection

All animal procedures were conducted in accordance with the Institutional Animal Care and Use Committee (IACUC) guidelines under protocol number 1509061B. We developed an inducible muscle-specific knockout model *Depdc5^{fl/fl} × Cre^{+/-}* (20). This model induces *Depdc5* deletion by Cre-loxP technology in mice that have tamoxifen-inducible Cre recombinase only in the skeletal muscle. To develop this model, our laboratory crossed Tg(ACTA1-cre/Esr1*)2Ker/J (Cre) (RRID:IMSR_JAX:025750, Jackson Laboratory) with a homozygote floxed *Depdc5^{fl/fl}* mouse [officially, *Depdc5^{tm1c(EUCOMMHmgw)}*]. We used a total of 60 mice (4 groups) with an equal number of males and females per group. The group size was selected based on the previous studies from our group. Groups included C57BL/6 (RRID:IMSR_JAX:000664, Jackson Laboratory) wild-type sedentary (WT Sed), DEPDC5 muscle-specific knockout sedentary (KO Sed) with C57BL/6 background, C57BL/6 wild-type exercise (WT Ex), and DEPDC5 muscle-specific knockout exercise (KO Ex) with C57BL/6 background. To confirm the genotype status of the mice, DNA was extracted from an ear punch and analyzed using RT-PCR (20). Once KO mice reached 6–8 mo of age, they were injected with tamoxifen (5 consecutive days, 75 mg/kg), a Cre recombinase system inducer, to facilitate *Depdc5* deletion. In the previous study, we confirmed hyperactivation of mTORC1 after 6 wk of tamoxifen induction in the skeletal muscle of KO mice by measuring downstream targets of mTORC1 protein using Western blotting technique. Increased phosphorylation of downstream proteins in KO in comparison with WT mice indicated an overall increase in mTORC1 signaling in the skeletal muscle (20). Mice were group-housed (1–4 per cage) with their littermates in a temperature-controlled room with ad libitum access to food and water.

Exercise

Mice exercised on a motorized treadmill (PanLab LE 8710). They were acclimatized to the treadmill 1 day/week for 4 wk with the following protocols: *week 1*—5 min at 8 m/min; *week 2*—5 min at 8 m/min; *week 3*—30 min at 16 m/min; *week 4*—30 min at 16 m/min. In *week 5*, the mice underwent an acute bout of exercise, which consisted of 11-min warm-up run followed by a 60-min run at 16 m/min. Immediately after the completion of exercise, mice were anesthetized with a Ketamine/Xylazine mixture. Following deep anesthesia, quadriceps muscle tissue was isolated during a nonsurvival

surgery and flash-frozen in liquid nitrogen. All samples were stored at -80°C .

Metabolite Extraction from Skeletal Muscle

We extracted polar metabolites and lipids using a modified Bligh-Dyer extraction (22). Approximately 20 mg of muscle quadriceps tissue were added to a 1.5-mL Safe-Lock Eppendorf tube with enough 1.3-mm steel beads (BioSpec Corp.) to cover tissues. Prior to extraction, 10 μL of UltimateSPLASH ONE IS mix (Avanti Polar Lipids, Cat. No. 330820) diluted 1:5 in dichloromethane/methanol (1:1, vol/vol) and 10 μL of a polar metabolite IS mix prepared in 80% acetonitrile (composed of equal volumes of Carnitine/Acylcarnitine Standard Mix Set B, Cambridge Isotope Laboratories, Cat. No. NSK-B-1; Carnitine/Acylcarnitine Standard Mix Supplement to NSK-B, Cambridge Isotope Laboratories, Cat. No. NSK-B-G1; Metabolomics QC Kit, Cambridge Isotope Laboratories, Cat. no. MSK-QC-KIT; and Organic Acid Mix, Cambridge Isotope Laboratories, Cat. No. MSK-OA-1) were added to samples to be used for normalization. About 300 μL of methanol/water (2:1.8, vol/vol) were added, and samples were homogenized using a bead homogenizer in 30-s pulses for two times. If tissues were not fully disrupted, samples were homogenized for another 30 s. Homogenates were then transferred to 12 \times 75 mm glass tubes. The emptied homogenate tubes were rinsed with 610 μL of methanol/water (2:1.8, vol/vol) two times, with the resulting rinse pooled with the homogenate. About 800 μL of chloroform were added to samples, followed by vortexing to mix and incubation on ice for 1 h. Following incubation, samples were centrifuged to separate the two phases; 1.3 mL of the upper aqueous phase were transferred to a new glass tube and dried through speedvac (Jouan RC 10.22 vacuum centrifuge). This fraction represented to polar metabolites. From the lower organic phase, 760 μL were transferred to a new tube and dried under a stream of nitrogen gas (Organomation Microvap). This fraction represented the lipids. The remaining protein pellet was used to determine the protein content through a BCA protein assay (Pierce BCA Assay Kit, Thermo Scientific). The polar metabolite extracts were resuspended in 100 μL of 80% acetonitrile following drying, whereas the lipid extracts were resuspended in 100 μL of dichloromethane/methanol (1:1, vol/vol).

LC-MS/MS Analysis

LC-MS/MS analysis for polar metabolites was performed using a 1260 Infinity UHPLC System (Agilent) coupled to a Turbo V electrospray ionization (ESI) source and a Qtrap 6500 mass spectrometer (SCIEX). In brief, the samples were separated in HILIC mode using an Atlantis Premier BEH Z-Hilic column (2.5 μm , 2.1 \times 150 mm, Waters). Mobile phase A consisted of acetonitrile/water (10:90, v/v) + 10 mM ammonium acetate + 2.5 μM InfinityLab deactivator agent (Agilent), pH 9.0; and mobile phase B consisted of acetonitrile/water (90:10, v/v) + 10 mM ammonium acetate + 2.5 μM InfinityLab deactivator agent (Agilent), pH 9.0. All solvents were LCMS grade. The LC gradient was as follows: 0–2 min, 15% A; 2–6 min, 15% to 70% A; 6–15 min, 70% to 85% A; 15–16 min 85% to 95% A; 16–20 min, 95% A; 20–22 min, 95 to 15% A; 22–32 min, 15% A. The flow rate was 200 $\mu\text{L}/\text{min}$, and the column temperature was 35°C . Ten microliters of samples were injected. Polar metabolites were analyzed

using scheduled multiple reaction monitoring (sMRM) for a total of 274 metabolites. The ESI source parameters were set as follows: curtain gas (CUR) at 25 psi, collision activated dissociation (CAD) set to high temperature of 475°C , nebulizing gas (GS1) and heating gas (GS2) at 35 psi, and ionspray voltage at 4,500 V in positive ionization mode and $-4,500$ V in negative ionization mode. Lipids were analyzed using the same LC and mass spectrometer described earlier, using a method previously described (23). Samples were separated in HILIC mode using a Luna NH2 column (3 μm , 150 \times 4.6 mm, Phenomenex). Mobile phase A consisted of acetonitrile/water/hexane (92:6:2, vol/vol/vol) + 2 mM ammonium acetate, pH 9.3, and mobile phase B consisted of acetonitrile/water (50:50, vol/vol) + 2 mM ammonium acetate, pH 9.3. The gradient was as follows: 0–2 min, 100% A; 2–6.5 min, 100% to 60% A; 6.5–7 min, 60% to 55% A; 7–9 min, 55% A; 9–9.5 min, 55% to 30% A; 9.5–12 min, 30% A; 12–12.1 min, 30% to 15% A; 12.1–14.5 min, 15% A; 14.5–14.6 min, 15% to 0% A; 14.6–17 min, 0% A; 17–18.1 min, 0% to 100% A; 18.1–22 min, 100% A. The flow rate was 1 mL/min, column temperature was 35°C , and the injection volume was 5 μL . Lipids were also analyzed using sMRM for a total of 1,870 lipid species across 18 lipid classes. The ESI source parameters were set as follows: CUR set to 30 psi, CAD set to medium, temperature set to 450°C , GS1 set to 50 psi, GS2 set to 55 psi, and ionspray voltage set to 5,500 V in positive ionization mode and $-4,500$ V in negative ionization mode.

Data Processing and Statistical Analysis

Peak areas for metabolites and lipids were normalized to peak areas of the relevant internal standards and the sample protein concentration. Analyst software (V. 1.7, Sciex) was used to operate the LC-MS instrument and acquire data. Skyline software 22.2 (RRID:SCR_014080) was used for peak picking and exporting sample data. Multivariate and univariate statistical analyses were performed using Metaboanalyst 6.0 (RRID:SCR_015539) (24), including principal component analysis (PCA) and pathway analysis (KEGG [RRID:SCR_012773] database). Two-way ANOVA and Games–Howell post hoc tests were used to analyze differences between groups with P and P -adjusted [False Discovery Rate (FDR)] < 0.05 (Benjamini–Hochberg correction). Volcano plots were created between sample groups with thresholds of P and P -adjusted < 0.05 . Heatmaps were created based on relative fold change and P values.

RESULTS

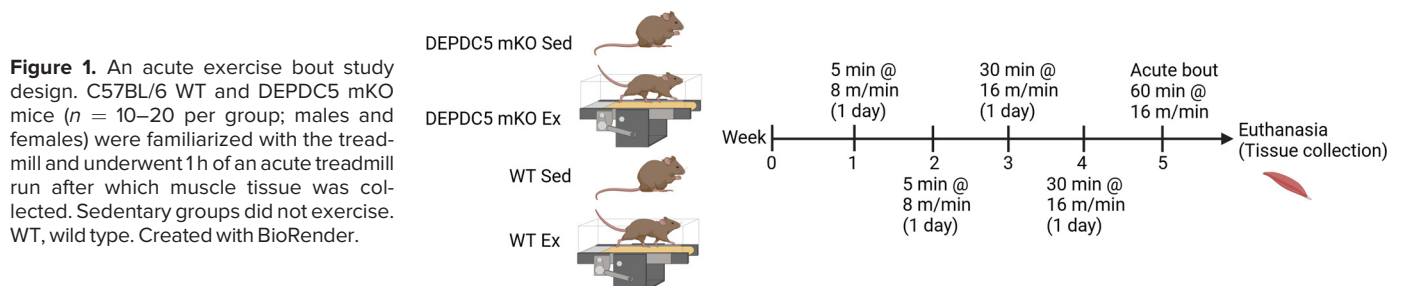
The Effect of Exercise on Metabolic Responses (Sedentary vs. Postexercise)

WT and DEPDC5 mKO mice exercised for 60 min at 16 m/min on a motorized treadmill. There was no difference in exercise performance between both groups. First, we examined mTORC1 activation in skeletal muscle to confirm the knockout status. Previous extensive work conducted in our laboratory validated the knockout status of our models (20). For this study, there was an overall increase in mTORC1 signaling in sedentary DEPDC5 mKO mice compared with WT Sed mice as indicated by a large increase in downstream

substrates p-4E-BP1 and p-rS6 (Supplemental Fig. S1). In contrast, we found a decrease in phosphorylated eukaryotic translation initiation factor 4E-binding protein 1 (p-4E-BP1) and an approaching significance increase in phosphorylated AMP-activated protein kinase (p-AMPK) in all exercising mice as compared with sedentary mice ($P < 0.07$ for WT and $P < 0.1$ for KO). To evaluate the exercise-induced changes in the skeletal muscle metabolome, we performed LC-MS/MS analysis following 1 h of an acute bout of treadmill exercise in WT and DEPDC5 muscle-specific KO mice (Fig. 1). Principal component analysis (PCA) (Fig. 2A) showed a large overlap between WT exercising (WT Ex) and WT sedentary (WT Sed) groups, indicating small differences between the two groups (Fig. 2A). To a similar extent, there was a large overlap between KO groups (Fig. 2B). There were nine significantly decreased and five significantly increased metabolites in WT Ex mice (P -adjusted < 0.05) (Fig. 2C). In contrast, KO Ex mice showed 8 significantly decreased and 12 increased metabolites (P -adjusted < 0.05) (Fig. 2D). There was no overlap in metabolites between two groups (Fig. 2E). The data displayed in the heatmap showed the WT group had increased metabolites related to lipid metabolism (octanoylcarnitine), organic acids (3-indolebutyric acid), and purines/pyrimidines (thymine, adenine, dGDP). In contrast, KO Ex mice had significantly increased metabolites related to nucleotide metabolism (dCTP, CTP, NAD, ADP, UDP-*N*-acetyl-glucosamine), organic acids (citraconic acid, maleic acid), glycolytic (glucose-6-phosphate), lipid metabolism (retinal), amino acids, and their derivatives (imidazole, *N*-alpha-acetyl-lysine) (Fig. 2F). There was a total of nine significantly decreased metabolites in WT Ex mice and eight metabolites in KO Ex mice (Fig. 2G). Top metabolites decreasing in WT Ex mice were related to nucleotide metabolism (UTP, methyl adenosine), TCA cycle (succinate), amino acid metabolism (sarcosine, imidazole), carbohydrate metabolism (glucosamine), metabolic regulation (methylmalonate), cofactors/vitamins (biotin), and citraconic acid (Fig. 2H). In contrast, KO Ex mice showed decreases in metabolites related to glycolysis (fructose 1,6-diphosphate and glycerol phosphate), organic acids (2-isopropylmalic acid and 3-indolebutyric acid), amino acid derivatives (aminobutyric acid), cholesterol metabolism (trimethylamine-*N*-oxide), and nucleotide metabolism (thymine and methylthioadenosine). Pathway analysis (Fig. 2I) indicated that most of the pathways were decreased in WT mice after exercise including TCA cycle, valine, leucine, and isoleucine degradation, and fatty acid metabolism. In turn, KO mice had significantly decreased pathways related to glycolysis/gluconeogenesis and PPP and increased lipid and pyrimidine metabolism.

The Effect of Genotype on Metabolic Responses

We also wanted to investigate the effect of the hyperactive mTORC1 genotype in the experiment relative to its corresponding exercise group (i.e., KO Sed vs. WT Sed and KO Ex vs. WT Ex) (Fig. 3). PCA showed a partial separation between WT Sed versus KO Sed (Fig. 3A) and a partial separation between KO Ex and WT Ex groups (Fig. 3B). A volcano plot indicated that more metabolites were decreased in KO Sed in comparison to WT Sed (Fig. 3C). In contrast, little fewer metabolites were decreased after exercise when comparing KO Ex versus WT Ex (Fig. 3D). When comparing the overlap in significantly decreased metabolites, we found 34 metabolites were unique to the KO Sed versus WT Sed comparison, 30 metabolites were unique to the KO Ex versus WT Ex comparison, and 18 were shared between the two group comparisons (P -adjusted < 0.05) (Fig. 3E). Heatmap data indicated that the top decreased metabolites in KO Sed relative to WT Sed were related to carbohydrate and energy metabolism (succinate, dihydroxyacetone phosphate, succinate, and methylmalonate), amino acids and their derivatives (1-methylhistidine), organic acids (maleic acid), and vitamin (riboflavin) (P -adjusted < 0.05) (Fig. 3F). In contrast, KO Ex mice showed significant decrease in amino acids and their derivatives (hydroxyproline, threonine, serine, isoleucine, and proline), nucleotides/nucleosides (thymine), vitamins and cofactors (pyridoxamine and riboflavin), trimethylamine-*N*-oxide, and 3-indolebutyric acid (P -adjusted < 0.05). There was a smaller number of significantly increased metabolites in both groups (Fig. 3G). It included 3-indolebutyric acid, octanoylcarnitine, and fructose 1,6-diphosphate for KO Sed, whereas KO Ex had alternations in nucleotide/nucleoside metabolism (methyl adenosine, UTP, and UDP), glucosamine, isovalerylcarnitine, biotin, and citraconic acid (Fig. 3H). Pathway analysis indicated a few distinct pathways that were unique for KO Sed and KO Ex comparisons. For example, KO Sed had significant decreases in glycolysis/gluconeogenesis, taurine, pentose phosphate pathway, pyruvate, and histidine metabolism compared with WT Sed. In contrast, KO Ex had decreases in linoleic acid, nicotinate and nicotinamide metabolism, arginine biosynthesis, tryptophan, and phenylalanine metabolism in comparison with WT Ex (Fig. 3I). In addition, we wanted to investigate the potential sex-based differences between exercising and nonexercising groups. Since males and females were analyzed separately, we assessed within-sex differences in response to exercise. We found that males exhibited significant changes in amino acids and their derivatives ($P < 0.05$) (Fig. 4A), whereas similar effects were not observed in females (Fig. 4B).



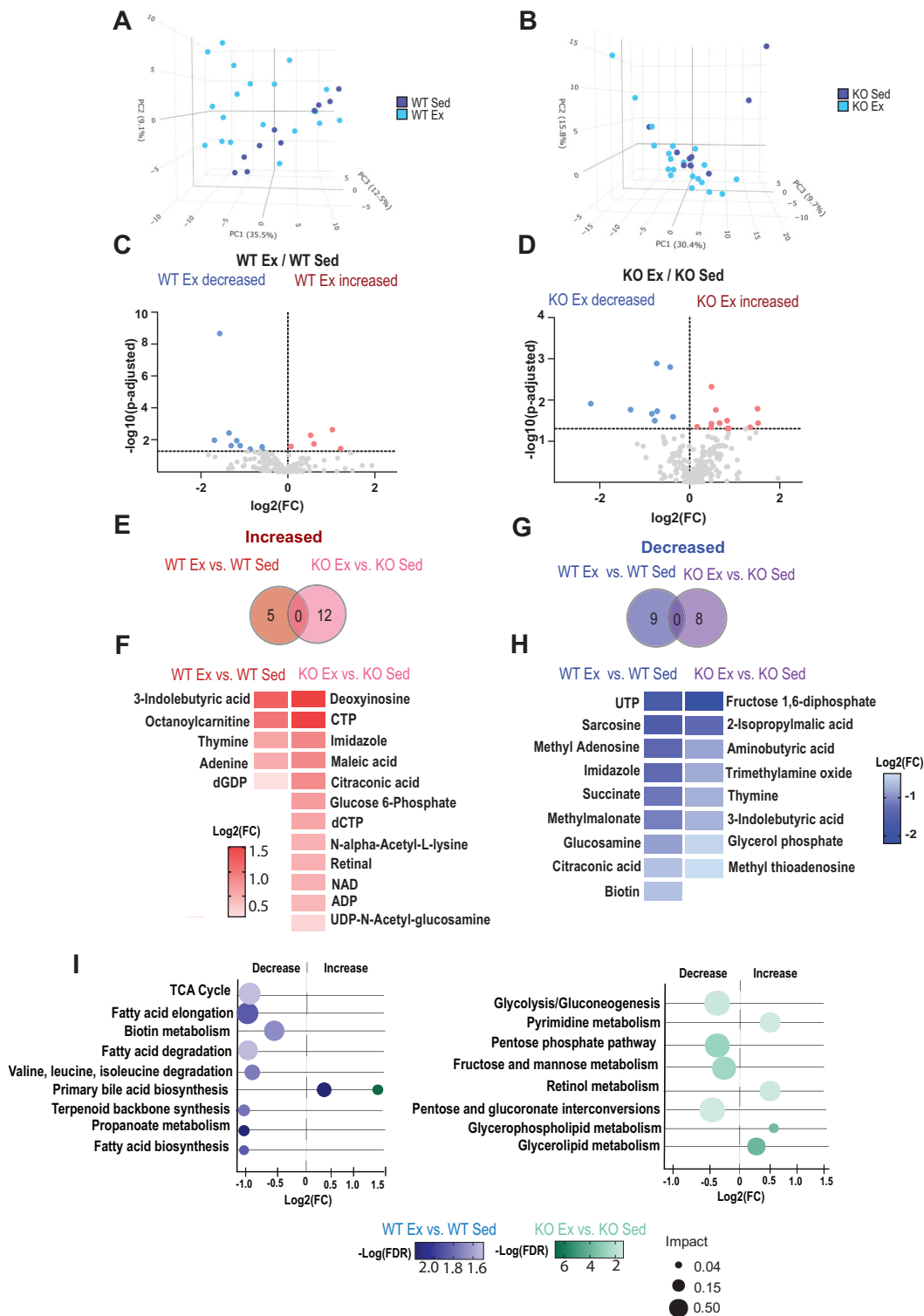


Figure 2. Metabolomics analysis of skeletal muscle at rest and after 1 h of treadmill exercise. Pairwise comparisons based on exercise (WT Ex vs. WT Sed and KO Ex vs. KO Sed). *A* and *B*: 3-D PCA plot of WT Ex and WT Sed (*A*) and KO Ex and KO Sed (*B*). *C* and *D*: volcano plot of increased (red) and decreased (blue) metabolites (*P*-adjusted < 0.05) for WT Ex and WT Sed (*C*) and KO Ex and KO Sed (*D*). *E*: Venn diagram of significantly increased metabolites (*P*-adjusted < 0.05) for WT Ex and WT Sed (red) and KO Ex and KO Sed (pink). *F*: top significantly increased metabolites (*P*-adjusted < 0.05). *G*: Venn diagram of significantly decreased metabolites (*P*-adjusted < 0.05) for WT Ex and WT Sed (blue) and KO Ex and KO Sed (purple). *H*: top significantly decreased metabolites (*P*-adjusted < 0.05). *I*: pathway analysis for WT Ex and WT Sed (blue) and KO Ex and KO Sed (green). Relative distribution of pathways according to their *P* values ($-\log[\text{FDR}]$) and relative impact from 0 (small) to 1 (large). Log₂(FC) indicates pathway fold change. For all analyses, data were pooled from both males and females (*n* = 10–20 per group). 3-D, three-dimensional; EX, exercising; KO, knockout; PCA, principal component analysis; SED, sedentary; WT, wild type.

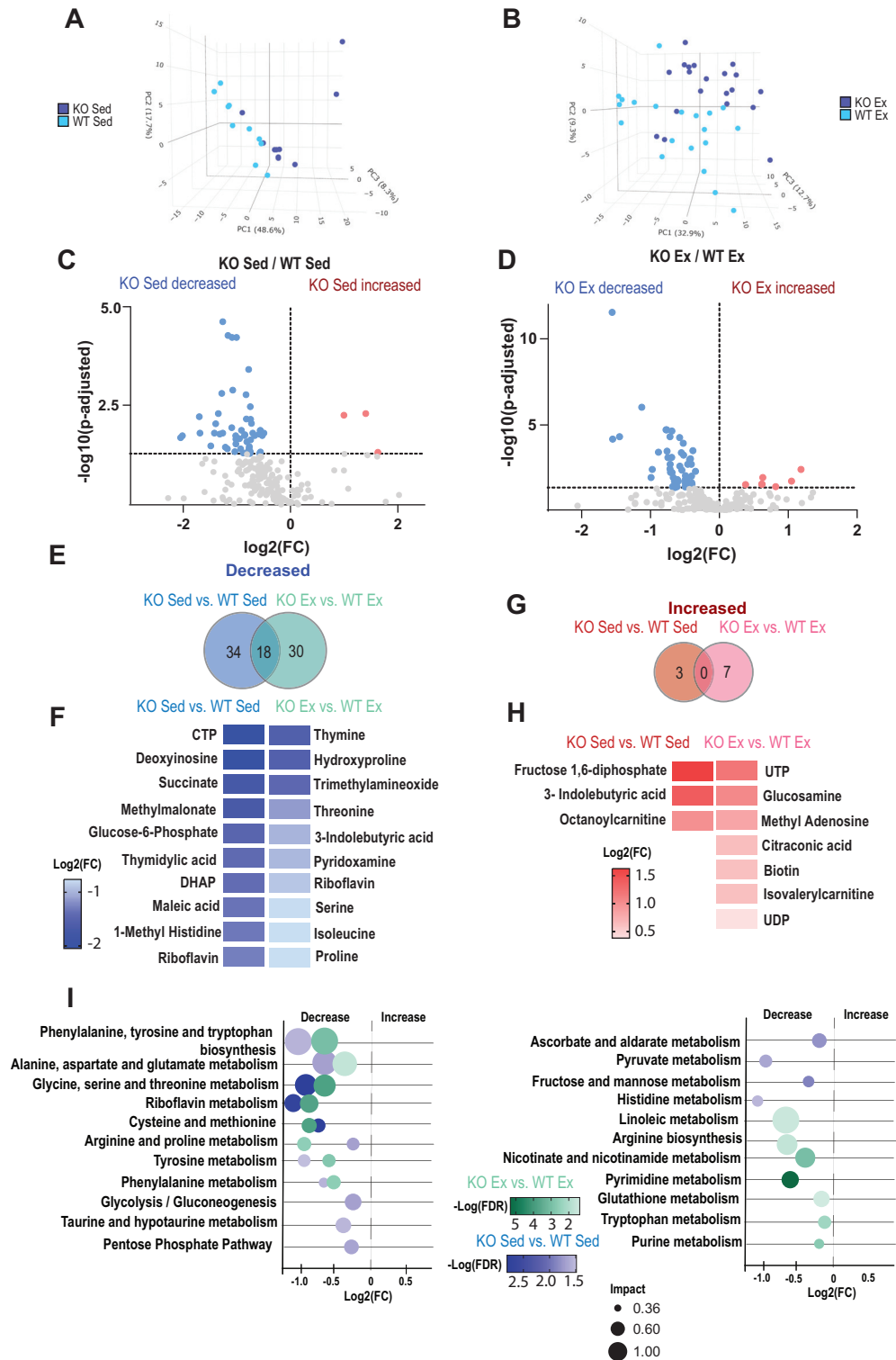


Figure 3. Metabolomics analysis of skeletal muscle at rest and after 1 h of treadmill exercise. Pairwise comparisons based on genotype (KO Sed vs. WT Sed and KO Ex vs. WT Ex). **A** and **B**: 3-D PCA plot of KO Sed and WT Sed (**A**) and KO Ex and WT Ex (**B**). **C** and **D**: volcano plot of increased (red) and decreased (blue) metabolites (P -adjusted < 0.05) for KO Sed and WT Sed (**C**) and KO Ex and WT Ex (**D**). **E** and **G**: Venn diagram of significantly decreased and increased metabolites (P -adjusted < 0.05) for KO Sed and WT Sed (green and red) and KO Ex and WT Ex (blue and pink). **F** and **H**: top significantly different metabolites (P -adjusted < 0.05). **I**: pathway analysis for KO Sed and WT Sed (blue) and KO Ex and WT Ex (green). Relative distribution of pathways according to their P values [$-\log(\text{FDR})$] and relative impact from 0 (small) to 1 (large). $\text{Log}_2(\text{FC})$ indicates pathway fold change. For all analyses, data were pooled from both males and females ($n = 10\text{--}20$ per group). 3-D, three-dimensional; EX, exercising; KO, knockout; PCA, principal component analysis; SED, sedentary; WT, wild type.

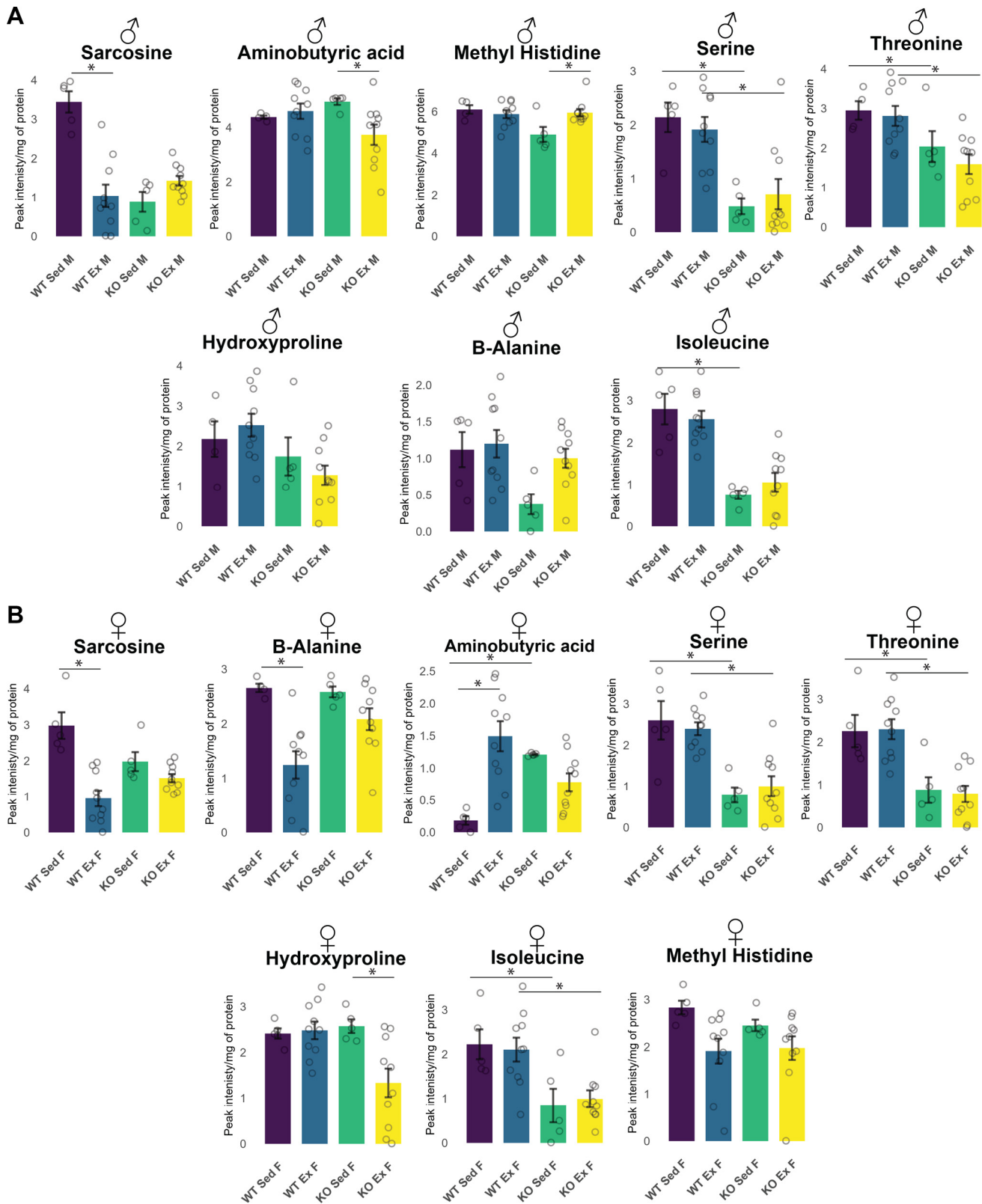


Figure 4. Sex-specific responses in amino acids and their derivatives. A: bar plots indicating differences in amino acids and their derivatives in males (A) and females (B). Data were stratified by sex ($n = 5-10$ per group), and separate two-way ANOVAs were performed (means \pm SE, $*P < 0.05$).

The Effect of Exercise on Lipidomic Responses (Sedentary vs. Postexercise)

Lipidomic analysis of the skeletal muscle tissues detected 1,092 lipid species (Fig. 5A). PCA of the lipidomic data from either the WT Sed versus WT Ex comparison or the KO Sed versus KO Ex comparison showed a partial separation, indicating small differences between the lipid profiles (Fig. 5, B and C). Volcano plot data indicated that 17 lipids were increased and 13 decreased in WT Ex mice relative to WT Sed, whereas 37 lipids were increased and 11 decreased in KO Ex mice relative to KO Sed ($P < 0.05$) (Fig. 5, D–F and I). The increased lipids were unique to either of the WT or KO comparisons (Fig. 5F). Phosphatidylglycerols (PGs), TGs, and phosphatidylcholines (PCs) were among the most altered lipid classes in WT after exercise (Fig. 5G), whereas TGs and PGs had the highest number of increased lipid species in KO mice after exercise. Data displayed in the heatmap indicated that the lipids with the greatest increases for WT Ex versus WT Sed were a cholesterol ester (CE), PGs (38–42 total carbons), TGs (50–54 total carbons), and PIs (39 total carbons) (Fig. 5H). In contrast, KO Ex mice showed increases in ceramide (20:1) (Cer), hexosylceramides (HexCers), dihydroceramides (dCers), PGs, DGs (36–38 total carbons), and TGs (Fig. 5H). There was a total of 11 unique lipids that decreased in WT Ex mice and 9 in KO Ex mice (Fig. 5I). CEs, DGs, and PGs were the top decreasing lipids in WT Ex mice (Fig. 5J), whereas PCs were the top decreasing lipids in KO after exercise (Fig. 5J). Heatmap data indicated that WT Ex mice showed the greatest reductions in PGs with 36–37 total fatty acid carbons, DGs with 32–36 total fatty acid carbons, and CEs with 16–18 fatty acid carbons (Fig. 5K). In contrast, KO mice showed the greatest decreases in PCs and PIs (Fig. 5K).

The Effect of Genotype on Lipidomic Responses

Similar to the metabolomic comparisons, we wanted to investigate the effect of genotype during exercise on the lipidomic profile (Fig. 6). PCA showed partial separation between WT Sed and KO Sed mice (Fig. 6A) and between WT Ex and KO Ex mice but to a lesser extent (Fig. 6B). A volcano plot indicated that 198 lipids were significantly decreased and 6 increased in KO Sed in comparison with WT Sed ($P < 0.05$) (Fig. 6C). In contrast, 145 lipids were decreased and 33 increased in KO Ex mice ($P < 0.05$) (Fig. 6D). All lipids shown to be increased for either the sedentary or the exercise group comparison were unique to those comparisons (Fig. 6E). TGs and plasmalogen phospholipids (PE-Ps) were mostly altered in KO Sed in comparison with WT Sed (Fig. 6F). In contrast, multiple classes including PGs, DGs, PEs, and PCs were the top increased lipids in KO Ex in comparison with WT Ex (Fig. 6F). Heatmap indicated that the top increased lipids for KO Sed in comparison with WT Sed were TGs with 50–54 total carbons and 1–3 double bonds and PE-Ps with 40–41 carbons (Fig. 6G). In contrast, KO Ex versus WT Ex had mostly altered DGs with 33–36 total carbons, Cers with 20–24 total carbons, and PGs with 33–44 total carbons (Fig. 6G). There was a total of 167 unique decreased lipids in KO Sed in comparison with 114 in KO Ex mice (Fig. 6H). The lipid classes showing the largest decreases in KO Sed versus WT Sed were TGs

and DGs (Fig. 6I). In contrast, PCs and TGs were the most decreased lipids in KO Ex (Fig. 6J). Heatmap data showed that TGs with 52–60 carbons were the most altered in KO Sed versus WT Sed, whereas PGs (38–42 total carbons) and TGs with 52–60 carbons were the most reduced in KO Ex versus WT Ex (Fig. 6J).

We also wanted to determine sex-specific differences in the muscle lipidome between WT and KO after one bout of exercise. We stratified data by sex and found males having exercise-specific differences in PS, PI, PG, SM, Cer, and dCer lipid classes ($P < 0.05$) (Fig. 7A). In contrast, within-group comparisons in females had significant exercise-specific differences in PSs and dCers (Fig. 7B).

DISCUSSION

In this study, we investigated the effect of 1 h of an acute bout of treadmill exercise on muscle metabolomic and lipidomic profile in mice with hyperactive muscle mTORC1. KO mice showed decreases in metabolites in pathways related to glycolysis and pentose phosphate pathway and increase in nucleotide and lipid metabolism intermediates. In contrast, WT mice primarily showed decreases in TCA cycle and fatty acid metabolism intermediates. In terms of specific lipid classes, KO Ex mice showed an increased turnover of TGs. Conversely, WT Ex mice showed differences in multiple lipid classes, but to a smaller extent. Genotype had a larger effect than exercise in both skeletal muscle metabolome and lipidome, with sedentary mice experiencing the most significant changes, which decreased following exercise. We also observed within-sex differences in the muscle metabolome and lipidome with males and females having unique alterations in amino acids and their derivatives and males revealing increases in SM, Cer, PG, PI, and PS lipid classes. These findings highlight that mTORC1 hyperactivation profoundly alters muscle metabolism with a greater impact than the effect of an acute exercise alone, while still driving unique metabolic changes in response to exercise stress.

Regarding the overall fuel utilization during exercise, pathway analysis revealed significant decrease in TCA cycle metabolites for WT mice, whereas KO mice exhibited significant decrease in glycolytic metabolites, indicating distinct patterns of fuel utilization. During prolonged moderate-intensity exercise, fuel usage shifts toward aerobic metabolism with carbohydrates and fats having similar relative contribution (25), which leads to greater reliance on the TCA cycle and oxidative phosphorylation pathways (11). In our study, WT mice had a decrease in TCA cycle metabolites indicating an exercise-induced shift toward oxidative metabolism. In the context of mTORC1 hyperactivation and fuel usage, previous studies showed that *Tsc1*^{-/-} and *Tsc2*^{-/-} cells, which result in constitutively active mTORC1, exhibit increased expression of glycolytic enzymes and an increased reliance on glycolysis (26). Another study demonstrated that similar knockout models of hyperactive mTORC1 had increased glucose consumption and lactate production, which was reversed by rapamycin treatment (27). These findings support our observations of increased reliance on glycolysis in both sedentary and exercised mice with hyperactive mTORC1 and suggest that these mice sustain a preference for nonoxidative glucose metabolism, potentially impairing

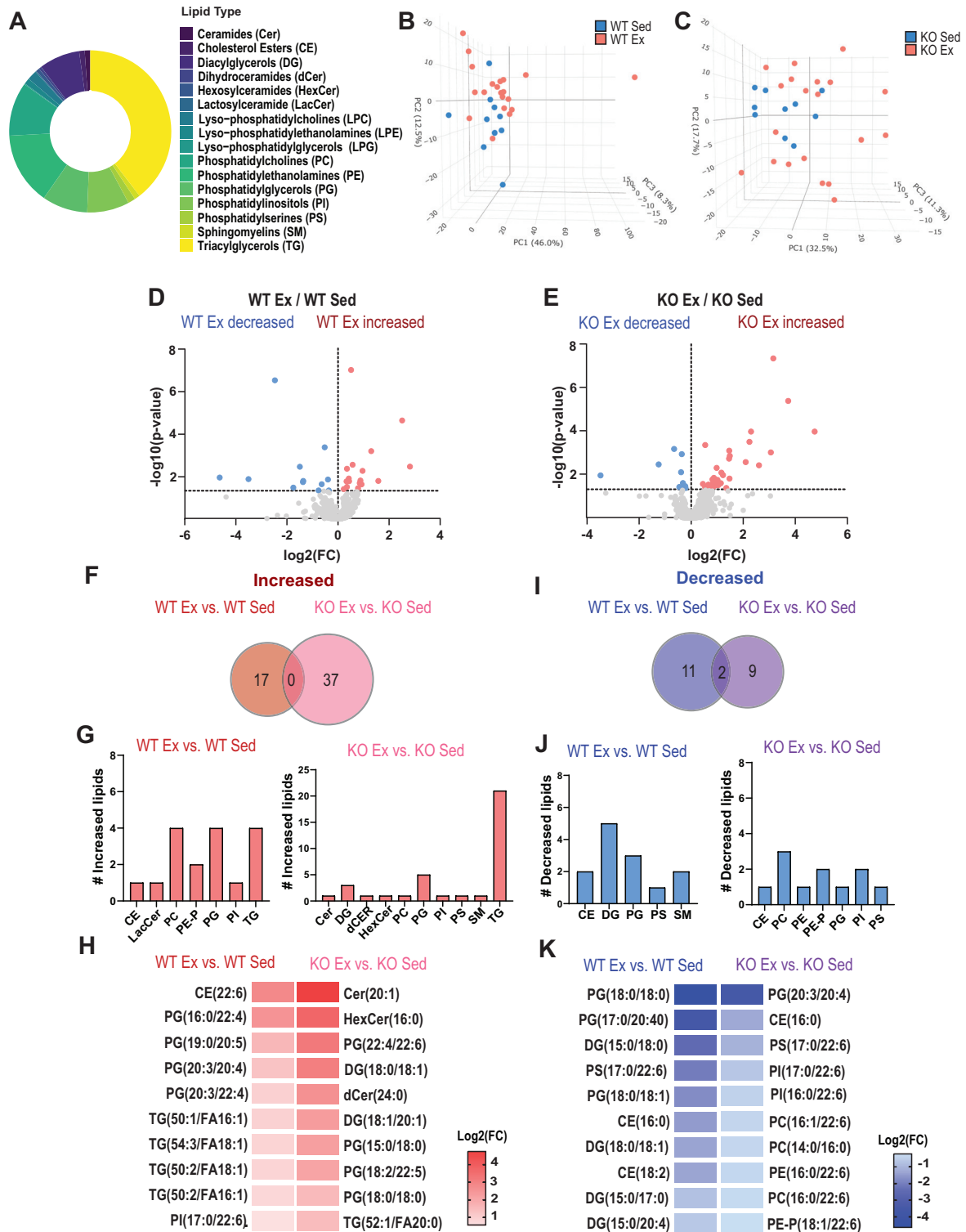


Figure 5. Lipidomics analysis of skeletal muscle at rest and after 1 h of treadmill exercise. Pairwise comparisons based on exercise (WT Ex vs. WT Sed and KO Ex vs. KO Sed). **A:** pie chart of uniquely identified lipid species within each lipid class. **B** and **C:** 3-D PCA plot of WT Ex and WT Sed (**B**) and KO Ex and KO Sed (**C**). **D** and **E:** volcano plot of uniquely increased (red) and decreased (blue) metabolites (P -adjusted < 0.05) for WT Ex vs. WT Sed (**D**) and KO Ex vs. KO Sed (**E**). **F:** Venn diagram of significantly increased metabolites (P -adjusted < 0.05) for WT Ex vs. WT Sed (red) and KO Ex vs. KO Sed (pink). **G:** bar plots of the total number of increased lipids. **H:** top 10 significantly increased metabolites (P -adjusted < 0.05). **I:** Venn diagram of significantly decreased metabolites (P -adjusted < 0.05) for WT Ex and WT Sed (purple) and KO Ex and KO Sed (blue). **J:** bar plots of the total number of decreased lipids. **K:** top 10 significantly decreased metabolites (P -adjusted < 0.05) for WT Ex and WT Sed and KO Ex and KO Sed. For all analyses, data were pooled from both males and females ($n = 10$ – 20 per group). 3-D, three-dimensional; EX, exercising; KO, knockout; PCA, principal component analysis; SED, sedentary; WT, wild type.

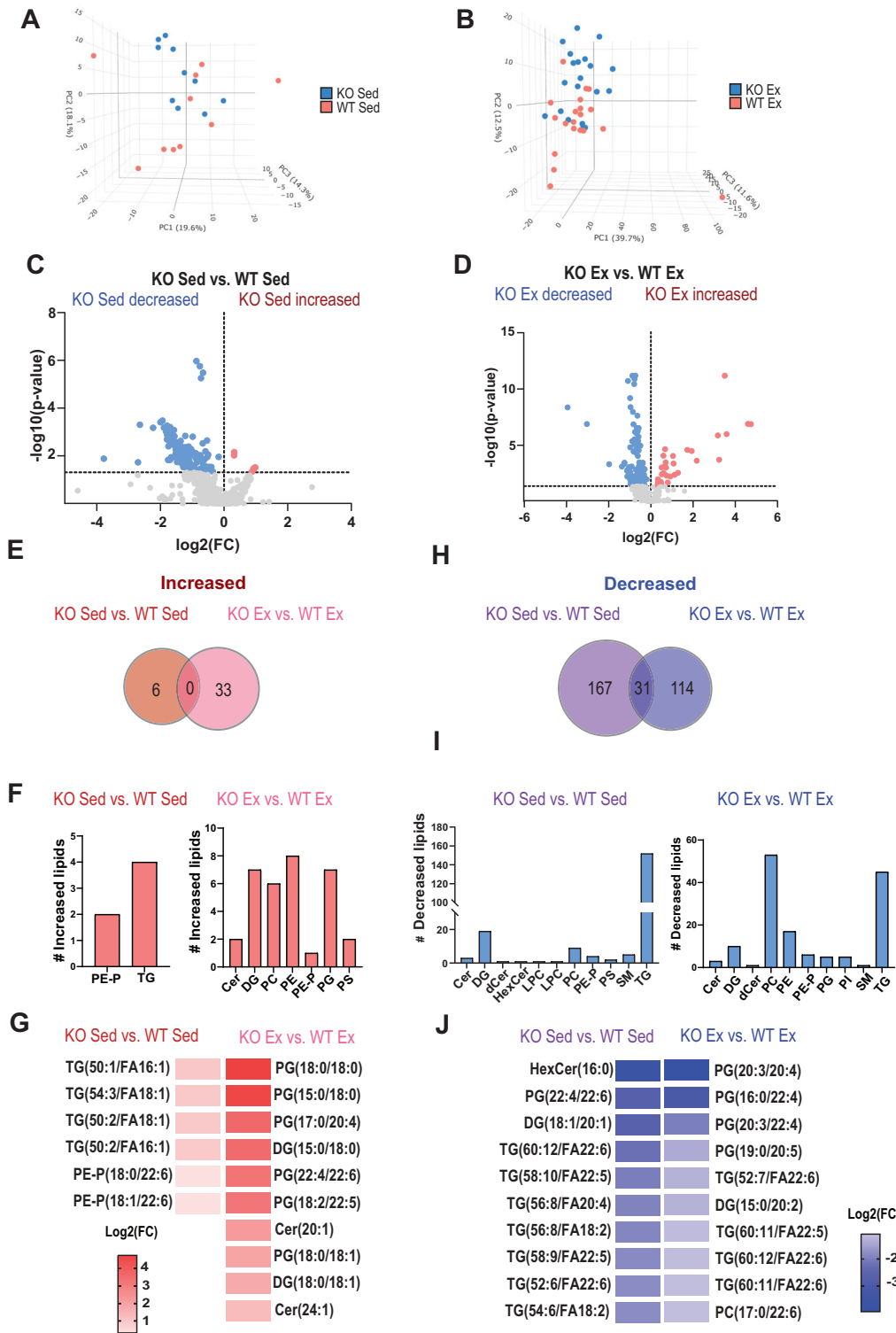


Figure 6. Lipidomics analysis of skeletal muscle at rest and after 1 h of treadmill exercise. Pairwise comparisons based on genotype (KO Sed vs. WT Sed and KO Ex vs. WT Ex). *A* and *B*: 3-D PCA plot of KO Sed and WT Sed (*A*) and KO Ex and WT Ex (*B*). *C* and *D*: volcano plot of increased (red) and decreased (blue) metabolites (P -adjusted < 0.05) for KO Sed and WT Sed (*C*) and KO Ex and WT Ex (*D*). *E*: Venn diagram of significantly increased metabolites (P -adjusted < 0.05) for KO Sed and WT Sed (red) and KO Ex and WT Ex (pink). *F*: bar plots of the total number of increased lipids. *G*: top 10 significantly increased metabolites (P -adjusted < 0.05). *H*: Venn diagram of significantly decreased metabolites (P -adjusted < 0.05) for KO Sed and WT Sed (purple) and KO Ex and WT Ex (blue). *I*: bar plots of the total number of decreased lipids. *J*: top 10 significantly decreased metabolites (P -adjusted < 0.05). For all analyses, data were pooled from both males and females ($n = 10-20$ per group). 3-D, three-dimensional; EX, exercising; KO, knockout; PCA, principal component analysis; SED, sedentary; WT, wild type.

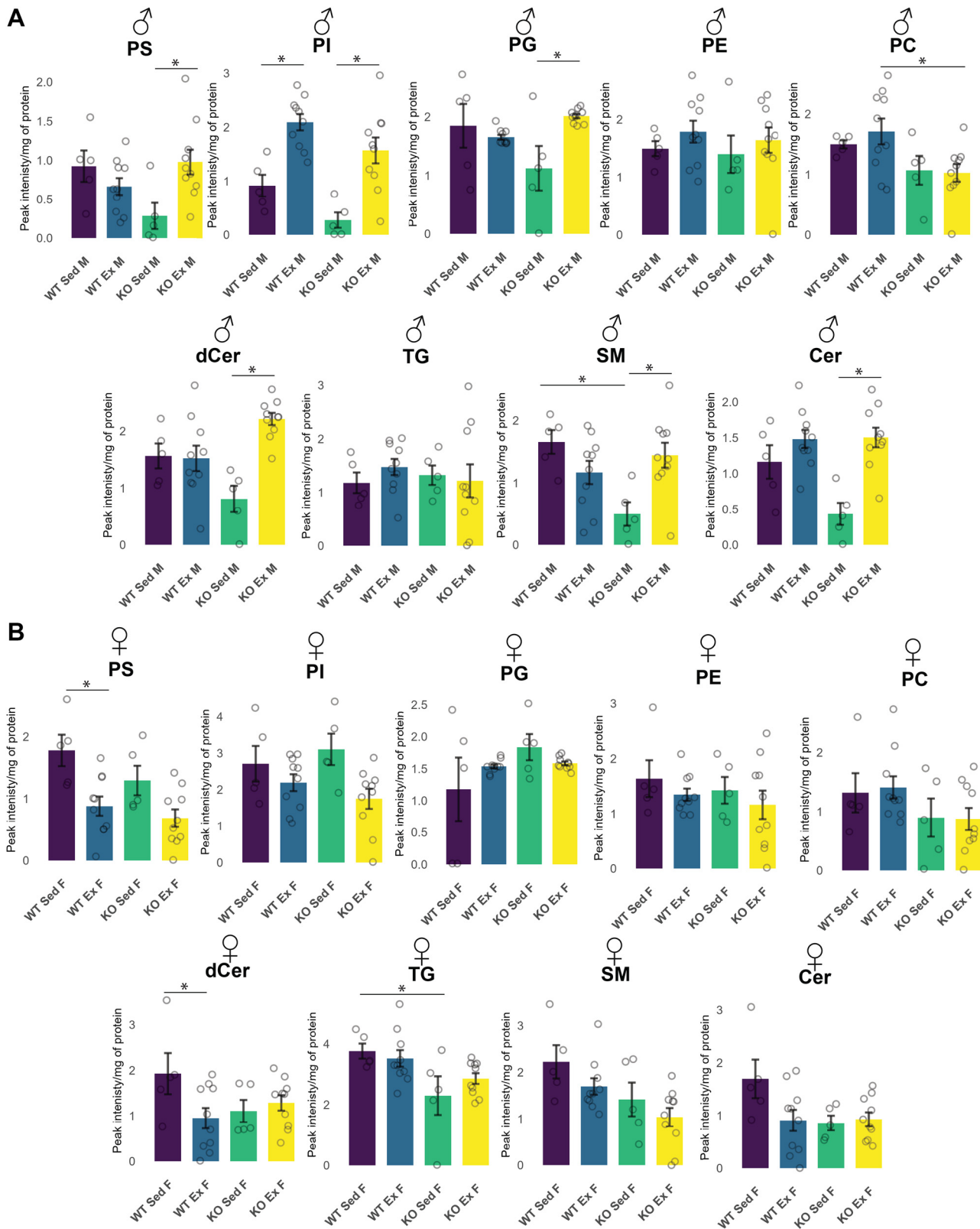


Figure 7. Sex-specific lipidomic responses. Bar plots indicating average lipid intensity in males (A) and females (B). Data were stratified by sex, and separate two-way ANOVAs were performed. Reported means \pm SE, * $P < 0.05$; $n = 5-10$ per group.

the ability to transition to oxidative metabolism even during prolonged exercise.

Exercise caused a significant increase in intermediate metabolites of pyrimidine metabolism in KO mice. Regarding exercise-induced changes, although two studies reported an increase in degradation of pyrimidine metabolites (28, 29), there is a lack of studies that investigated the impact of exercise on pyrimidine metabolism. Our finding is consistent with the stimulated pyrimidine synthesis with activated mTORC1 in cells (30). These changes indicate that KO mice with hyperactive mTORC1 may rely more on nucleotide synthesis to support the increased anabolic demands induced by both mTORC1 activation and exercise, rather than relying on nucleotide degradation.

We also found exercise-induced decrease in metabolites in PPP in KO mice. Similarly, Düvel et al. (26) reported activation of PPP genes and increase in pathway flux in cells with hyperactive mTORC1. Although it is unclear whether exercise in animals stimulates PPP, one study reported that high-frequency electrical stimulation of C2C12 myotubes upregulated gene expression and metabolites in PPP through ROS-dependent activation (31). Combining these findings, similar to glycolytic changes, it may suggest an increased utilization of PPP pathway during exercise in the muscle of mice with hyperactive mTORC1 that serves potentially as an adaptive mechanism to manage oxidative stress and demands for nucleotide synthesis.

There are few studies that have examined the effect of acute exercise on the skeletal muscle lipidome. Our study revealed exercise-induced distinct lipidomic profiles between WT and KO mice. Notably, KO mice had a higher number of uniquely increased lipids postexercise compared with WT mice. In WT mice, exercise led to small turnover in multiple lipid classes including DG, TG, and PG, which are key components in cellular energy storage and signaling. Conversely, we observed a large increase of TGs in KO mice. Studies examining the effect of exercise on lipids in skeletal muscle found an increase in intramuscular triglycerides (IMTG) utilization with exercise in humans (19, 32). This decrease in IMTG can be attributed to the breakdown of TGs into DGs, free fatty acids (FFAs), and glycerol (32). FFAs can then be used for beta-oxidation, providing a primary source of fuel in the form of ATP needed for skeletal muscle contraction during prolonged exercise. mTORC1 controls de novo lipid synthesis by regulating the activation state of sterol regulatory element-binding protein 1 (SREBP-1) in liver and adipose tissue (33), although its role in skeletal muscle is unclear. The increased number of TGs in our study in KO mice, in addition to an increased reliance on the glycolytic pathway, after exercise may indicate a reduced reliance on oxidative metabolism.

Cers, sphingolipid derivatives, play a role in apoptosis, cell growth arrest, differentiation, and senescence (34). They are implicated in the pathogenesis of diabetes and insulin resistance. An increase in Cers in a lipotoxic environment may contribute to the development of insulin resistance in the skeletal muscle (35). In the context of acute exercise, one study reported a decrease in Cers in humans performing moderate-intensity exercise for 90 min (32). Another study examined nine intramuscular ceramides (C14:0 to C24:1) in young and old adults after an acute bout of resistance exercise (36).

Although they did not find significant differences in ceramides before and after exercise, older individuals had significantly higher Cers as compared with young individuals. In our study, when analyzed males and females separately, we found males had a significant increase in Cers, in KO mice postexercise, and both males and females had Cer 18:1;O2/20:1 levels increasing 28-fold. Cers have been found to inhibit the Akt pathway, an upstream regulator of mTORC1, which suggests potential modulation of mTORC1 activity (37). In the context of hyperactive mTORC1 and exercise, the interplay between increased exercise-induced oxidative stress and inflammation, enhanced lipolysis, and a feedback inhibition of Akt signaling pathway may be responsible for the increased Cers in KO mice with hyperactive mTORC1 after exercise.

We observed an increased turnover of PGs in both WT and KO mice in response to exercise. PGs are important structural components of mitochondrial membrane and mediators of molecular signaling (38). These changes in PGs content may be caused by exercise-induced changes in mitochondrial membrane remodeling due to an increase in energy demands.

Our study demonstrates that hyperactive mTORC1 as induced by the skeletal muscle-specific knockout of DEPDC5 exhibited greater changes in the muscle metabolome and lipidome compared with the effects of exercise alone. Metabolites and lipids were predominantly decreased in KO mice in the sedentary state relative to WT mice. During exercise, there were fewer significantly changing metabolites, suggesting a potential compensatory effect of exercise in restoring metabolic homeostasis. In terms of lipids, sedentary KO mice compared with WT mice had a large decrease in TGs and DGs, whereas exercising KO mice had a decrease in TGs and PCs.

Our findings reveal significant alterations in the metabolomic and lipidomic profile of mice with hyperactive muscle mTORC1 following 1 h bout of exercise. Genotype had a much stronger impact than exercise alone, with predominantly decreased metabolites in sedentary mice that were partially restored with exercise. Prolonged acute exercise induced an increased reliance on glycolytic and PPP metabolites in the muscle of mice with hyperactive mTORC1, along with an increase in TGs. These findings suggest a reduced reliance on oxidative metabolism and a shift toward nonoxidative metabolism. Understanding the mechanisms of mTORC1 hyperactivation in the skeletal muscle and its impact on muscle metabolism and function could lead to the development of strategies for restoring mTORC1 signaling in aging and sarcopenia.

DATA AVAILABILITY

Data will be made available upon reasonable request.

SUPPLEMENTAL MATERIAL

Supplemental Fig. S1: <https://doi.org/10.6084/m9.figshare.28569170>.

ACKNOWLEDGMENTS

We thank the Mass Spectrometry Facility at the University of Texas Medical Branch (UTMB) for their invaluable support and assistance with the mass spectrometry analyses in this study. The

Graphical abstract and Fig. 1 were created using BioRender under an institutional license provided by UT Health San Antonio.

GRANTS

Funding for this study was provided by the following grants: NIA R56 AG051267, NIA P30 AG013319, and CPRIT RP190682.

DISCLOSURES

No conflicts of interest, financial or otherwise, are declared by the authors.

AUTHOR CONTRIBUTIONS

H.K. and B.B.R. conceived and designed research; H.K., S.P.K., E.D.M., and R.M. performed experiments; H.K., T.B.R., J.J.L., and W.R.K. analyzed data; H.K., T.B.R., J.J.L., W.K.R., and B.B.R. interpreted results of experiments; H.K. and T.B.R. prepared figures; H.K. drafted manuscript; H.K., S.P.K., T.B.R., E.D.M., R.M., J.J.L., W.K.R., and B.B.R. edited and revised manuscript; H.K., S.P.K., T.B.R., E.D.M., R.M., J.J.L., W.K.R., and B.B.R. approved final version of manuscript.

REFERENCES

- Saxton RA, Sabatini DM. mTOR signaling in growth, metabolism, and disease. *Cell* 168: 960–976, 2017 [Erratum in *Cell* 169: 361–371, 2017]. doi:10.1016/j.cell.2017.02.004.
- Liu GY, Sabatini DM. mTOR at the nexus of nutrition, growth, ageing and disease. *Nat Rev Mol Cell Biol* 21: 183–203, 2020 [Erratum in *Nat Rev Mol Cell Biol* 21: 246, 2020]. doi:10.1038/s41580-019-0199-y.
- Simcox J, Lamming DW. The central mTOR of metabolism. *Dev Cell* 57: 691–706, 2022. doi:10.1016/j.devcel.2022.02.024.
- Yoon MS, Choi CS. The role of amino acid-induced mammalian target of rapamycin complex 1(mTORC1) signaling in insulin resistance. *Exp Mol Med* 48: e201-e201, 2016. doi:10.1038/emm.2015.93.
- Bentzinger CF, Lin S, Romanino K, Castets P, Guridi M, Summermatter S, Handschin C, Tintignac LA, Hall MN, Rüegg MA. Differential response of skeletal muscles to mTORC1 signaling during atrophy and hypertrophy. *Skelet Muscle* 3: 6, 2013. doi:10.1186/2044-5040-3-6.
- Castets P, Lin S, Rion N, Di Fulvio S, Romanino K, Guridi M, Frank S, Tintignac LA, Sinnreich M, Rüegg MA. Sustained activation of mTORC1 in skeletal muscle inhibits constitutive and starvation-induced autophagy and causes a severe, late-onset myopathy. *Cell Metab* 17: 731–744, 2013. doi:10.1016/j.cmet.2013.03.015.
- Laplante M, Sabatini DM. mTOR signaling in growth control and disease. *Cell* 149: 274–293, 2012. doi:10.1016/j.cell.2012.03.017.
- Lo JH, U KP, Yiu T, Ong MT, Lee WY. Sarcopenia: current treatments and new regenerative therapeutic approaches. *J Orthop Translat* 23: 38–52, 2020. doi:10.1016/j.jot.2020.04.002.
- Tang H, Inoki K, Brooks SV, Okazawa H, Lee M, Wang J, Kim M, Kennedy CL, Macpherson PCD, Ji X, Van Roekel S, Fraga DA, Wang K, Zhu J, Wang Y, Sharp ZD, Miller RA, Rando TA, Goldman D, Guan KL, Shrager JB. mTORC1 underlies age-related muscle fiber damage and loss by inducing oxidative stress and catabolism. *Aging Cell* 18: e12943, 2019. doi:10.1111/acer.12943.
- Egan B, Zierath JR. Exercise metabolism and the molecular regulation of skeletal muscle adaptation. *Cell Metab* 17: 162–184, 2013. doi:10.1016/j.cmet.2012.12.012.
- Hargreaves M, Spriet LL. Skeletal muscle energy metabolism during exercise. *Nat Metab* 2: 817–828, 2020 [Erratum in *Nat Metab* 2: 990, 2020]. doi:10.1038/s42255-020-0251-4.
- Sato S, Dyar KA, Treebak JT, Jepsen SL, Ehrlich AM, Ashcroft SP, Trost K, Kunzke T, Prade VM, Small L, Basse AL, Schönke M, Chen S, Samad M, Baldi P, Barrés R, Walch A, Moritz T, Holst JJ, Lutter D, Zierath JR, Sassone-Corsi P. Atlas of exercise metabolism reveals time-dependent signatures of metabolic homeostasis. *Cell Metab* 34: 329–345.e8, 2022. doi:10.1016/j.cmet.2021.12.016.
- Schaefer PM, Huang J, Butic A, Perry C, Yardeni T, Tan W, Morrow R, Baur JA, Wallace DC. Nicotinamide riboside alleviates exercise intolerance in ANT1-deficient mice. *Mol Metab* 64: 101560, 2022. doi:10.1016/j.molmet.2022.101560.
- Hoene M, Li J, Li Y, Runge H, Zhao X, Häring HU, Lehmann R, Xu G, Weigert C. Muscle and liver-specific alterations in lipid and acyl-carnitine metabolism after a single bout of exercise in mice. *Sci Rep* 6: 22218, 2016. doi:10.1038/srep22218.
- Contrepois K, Wu S, Moneghetti KJ, Hornburg D, Ahadi S, Tsai MS, Metwally AA, Wei E, Lee-McMullen B, Quijada JV, Chen S, Christle JW, Ellenberger M, Balliu B, Taylor S, Durrant MG, Knowles DA, Choudhry H, Ashland M, Bahmani A, Enslin B, Amsallem M, Kobayashi Y, Avina M, Perelman D, Schüssler-Florenza Rose SM, Zhou W, Ashley EA, Montgomery SB, Chaib H, Haddad F, Snyder MP. Molecular choreography of acute exercise. *Cell* 181: 1112–1130, 2020. doi:10.1016/j.cell.2020.04.043.
- Hu C, Hoene M, Zhao X, Häring HU, Schleicher E, Lehmann R, Han X, Xu G, Weigert C. Lipidomics analysis reveals efficient storage of hepatic triacylglycerides enriched in unsaturated fatty acids after one bout of exercise in mice. *PLoS One* 5: e13318, 2010. doi:10.1371/journal.pone.0013318.
- Senoo N, Miyoshi N, Goto-Inoue N, Minami K, Yoshimura R, Morita A, Sawada N, Matsuda J, Ogawa Y, Setou M, Kamei Y, Miura S. PGC-1 α -mediated changes in phospholipid profiles of exercise-trained skeletal muscle. *J Lipid Res* 56: 2286–2296, 2015. doi:10.1194/jlr.M060533.
- Chen M, Zhou L, Chen S, Shangquan R, Qu Y, Sun J. Acute and chronic effects of high-intensity interval training (HIIT) on postexercise intramuscular lipid metabolism in rats. *Physiol Res* 70: 735–743, 2021. doi:10.33549/physiolres.934722.
- Stellingwerff T, Boon H, Jonkers RAM, Senden JM, Spriet LL, Koopman R, van Loon LJ. Significant intramyocellular lipid use during prolonged cycling in endurance-trained males as assessed by three different methodologies. *Am J Physiol Endocrinol Physiol* 292: E1715–E1723, 2007. doi:10.1152/ajpendo.00678.2006.
- Graber TG, Fry CS, Brightwell CR, Moro T, Maroto R, Bhattarai N, Porter C, Wakamiya M, Rasmussen BB. Skeletal muscle-specific knockout of DEP domain containing 5 protein increases mTORC1 signaling, muscle cell hypertrophy, and mitochondrial respiration. *J Biol Chem* 294: 4091–4102, 2019. doi:10.1074/jbc.RA118.005970.
- Maroto R, Graber TG, Romsdahl TB, Kudlicki A, Russell WK, Rasmussen BB. Metabolomic and lipidomic signature of skeletal muscle with constitutively active mechanistic target of rapamycin complex 1. *J Nutr* 153: 3397–3405, 2023. doi:10.1016/j.tjnut.2023.10.016.
- Bligh EG, Dyer WJ. A rapid method of total lipid extraction and purification. *Can J Biochem Physiol* 37: 911–917, 1959. doi:10.1139/o59-099.
- Romsdahl TB, Cocuron JC, Pearson MJ, Alonso AP, Chapman KD. A lipidomics platform to analyze the fatty acid compositions of non-polar and polar lipid molecular species from plant tissues: Examples from developing seeds and seedlings of pennycress (*Thlaspi arvense*). *Front Plant Sci* 13: 1038161, 2022. doi:10.3389/fpls.2022.1038161.
- Chong J, Xia J. MetaboAnalystR: an R package for flexible and reproducible analysis of metabolomics data. *Bioinformatics* 34: 4313–4314, 2018. doi:10.1093/bioinformatics/bty528.
- Romijn JA, Coyle EF, Sidossis LS, Gastaldelli A, Horowitz JF, Enderit E, Wolfe RR. Regulation of endogenous fat and carbohydrate metabolism in relation to exercise intensity and duration. *Am J Physiol Endocrinol Physiol* 265: E380–E391, 1993. doi:10.1152/ajpendo.1993.265.3.E380.
- Düvel K, Yecies JL, Menon S, Raman P, Lipovsky AI, Souza AL, Triantafellow E, Ma Q, Gorski R, Cleaver S, Vander Heiden MG, MacKeigan JP, Finan PM, Clish CB, Murphy LO, Manning BD. Activation of a metabolic gene regulatory network downstream of mTOR complex 1. *Mol Cell* 39: 171–183, 2010. doi:10.1016/j.molcel.2010.06.022.
- Sun Q, Chen X, Ma J, Peng H, Wang F, Zha X, Wang Y, Jing Y, Yang H, Chen R, Chang L, Zhang Y, Goto J, Onda H, Chen T, Wang MR, Lu Y, You H, Kwiatkowski D, Zhang H. Mammalian target of rapamycin up-regulation of pyruvate kinase isoenzyme type M2 is critical for aerobic glycolysis and tumor growth. *Proc*

- Natl Acad Sci USA* 108: 4129–4134, 2011. doi:10.1073/pnas.1014769108.
28. **Dudzinska W, Suska M, Lubkowska A, Jakubowska K, Olszewska M, Safranow K, Chlubek D.** Comparison of human erythrocyte purine nucleotide metabolism and blood purine and pyrimidine degradation product concentrations before and after acute exercise in trained and sedentary subjects. *J Physiol Sci* 68: 293–305, 2018. doi:10.1007/s12576-017-0536-x.
 29. **Yamamoto T, Moriwaki Y, Takahashi S, Tsutsumi Z, Yamakita J, Higashino K.** Effect of muscular exercise on the concentration of uridine and purine bases in plasma—adenosine triphosphate consumption-induced pyrimidine degradation. *Metabolism* 46: 1339–1342, 1997. doi:10.1016/s0026-0495(97)90241-9.
 30. **Ben-Sahra I, Howell JJ, Asara JM, Manning BD.** Stimulation of de novo pyrimidine synthesis by growth signaling through mTOR and S6K1. *Science* 339: 1323–1328, 2013. doi:10.1126/science.1228792.
 31. **Hoshino D, Kawata K, Kunida K, Hatano A, Yugi K, Wada T, Fujii M, Sano T, Ito Y, Furuichi Y, Manabe Y, Suzuki Y, Fujii NL, Soga T, Kuroda S.** Trans-omic analysis reveals ROS-dependent pentose phosphate pathway activation after high-frequency electrical stimulation in C2C12 myotubes. *iScience* 23: 101558, 2020. doi:10.1016/j.isci.2020.101558.
 32. **Schenk S, Horowitz JF.** Acute exercise increases triglyceride synthesis in skeletal muscle and prevents fatty acid-induced insulin resistance. *J Clin Invest* 117: 1690–1698, 2007. doi:10.1172/JCI30566.
 33. **Laplante M, Sabatini DM.** An emerging role of mTOR in lipid biosynthesis. *Curr Biol* 19: R1046–R1052, 2009. doi:10.1016/j.cub.2009.09.058.
 34. **Hannun YA, Obeid LM.** Principles of bioactive lipid signalling: lessons from sphingolipids. *Nat Rev Mol Cell Biol* 9: 139–150, 2008. doi:10.1038/nrm2329.
 35. **Bandet CL, Tan-Chen S, Bourron O, Le Stunff H, Hajduch E.** Sphingolipid metabolism: new insight into ceramide-induced lipotoxicity in muscle cells. *Int J Mol Sci* 20: 479, 2019. doi:10.3390/ijms20030479.
 36. **Rivas DA, Morris EP, Haran PH, Pasha EP, Morais Mda S, Dolnikowski GG, Phillips EM, Fielding RA.** Increased ceramide content and NFκB signaling may contribute to the attenuation of anabolic signaling after resistance exercise in aged males. *J Appl Physiol (1985)* 113: 1727–1736, 2012. doi:10.1152/jappphysiol.00412.2012.
 37. **Hyde R, Hajduch E, Powell DJ, Taylor PM, Hundal HS.** Ceramide down-regulates System A amino acid transport and protein synthesis in rat skeletal muscle cells. *Faseb J* 19: 461–463, 2005. doi:10.1096/fj.04-2284fje.
 38. **Morita S-y, Terada T.** Enzymatic measurement of phosphatidylglycerol and cardiolipin in cultured cells and mitochondria. *Sci Rep* 5: 11737, 2015. doi:10.1038/srep11737.